Assessment of blood oxygen saturation using photoacoustic technique

Ratan K. Saha, Subhajit Karmakar & Madhusudan Roy

Journal of Optics

ISSN 0972-8821

J Opt
DOI 10.1007/s12596-013-0123-3

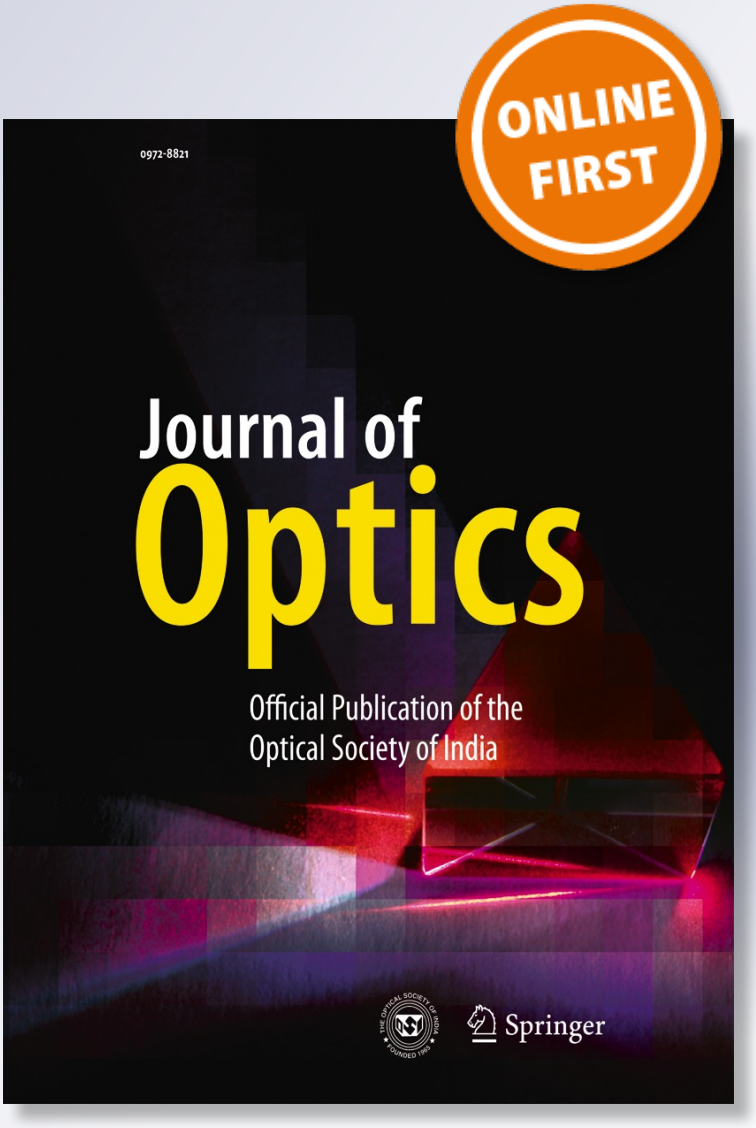

Springer

J Opt
DOI 10.1007/s12596-013-0123-3

RESEARCH ARTICLE

Assessment of blood oxygen saturation using photoacoustic technique

Ratan K. Saha · Subhajit Karmakar · Madhusudan Roy

Received: 16 December 2011 / Accepted: 18 January 2013

Abstract The accuracy of the photoacoustic (PA) technique to assess blood oxygen saturation (SO_2) using two laser beams was examined theoretically. A Monte Carlo technique was used to simulate 2D tissue configurations, and the PA signals from many red blood cells (RBCs) were constructed by summing the signals emitted by the individual cells. The level of oxygenation of each cell was assumed to be identical in a configuration. The cellular oxygenation state defined the blood SO_2 and also controlled the PA signal amplitude. The PA amplitude was observed to vary linearly with blood SO_2. It was nearly 4.6 times less and 8.2 times greater at $SO_2 = 100$ % than that of 0 % for the 600 and 1,064 nm incident optical radiations, respectively. The blood SO_2 was estimated using the PA amplitudes generated at these wavelengths. The estimated values agreed well with that of the actual SO_2 confirming the suitability of the PA technique to determine blood SO_2 noninvasively.

Keywords Photoacoustics · Optoacoustics · Blood oxygenation

Introduction

Invasive monitoring of cerebral blood oxygenation and brain tissue oxygenation is routinely performed in medical centres in developed countries and such information gathered is of vital importance to facilitate proper treatment. These examinations are carried out by using multiparameter sensor inserted into brain tissue, along with a standard ventriculostomy catheter and a microdialysis probe [1]. It is needless to say that noninvasive monitoring of blood oxygenation in different organs is very useful for the management of many life-threatening illnesses such as ischemia, sepsis, traumatic brain injury etc. [2, 3]. Although some efforts are made to engineer noninvasive monitors of brain oxygenation using near-infrared (near-IR) spectroscopy which utilizes the differences in optical absorption coefficients of oxyhemoglobin and deoxyhemoglobin, this technique suffers in terms of accuracy and depth monitoring since it accounts for strong light scattering and attenuation in the tissues [4–6]. Moreover, the development of near-IR monitoring of blood oxygenation is hindered as it encounters difficulties in esti-

The paper was part of a conference: contributed paper, published as part of the Proceedings of the 2nd International Conference on Trends in Optics and Photonics, Kolkata, India, December, 2011.

R. K. Saha (✉) · S. Karmakar · M. Roy
Saha Institute of Nuclear Physics, 1/AF Bidhannagar, Kolkata 700 064, India
e-mail: ratank.saha@saha.ac.in

M. Roy
e-mail: madhusudan.roy@saha.ac.in

Published online: 23 February 2013

mating the path length of scattered light through tissue [6].

In this context, it can be mentioned that the photoacoustic (PA) technique may serve in a better way as it can provide a real-time, noninvasive blood oxygenation monitoring method without the drawbacks as encountered in case of near-IR spectroscopy [2]. Based on this technique, quantification of oxygen in deep tissue regions can be made because oxygenation is estimated by analysing the pressure waves whose scattering in tissue is two to three orders of magnitude weaker than the optical scattering, thus resulting in less attenuation and greater penetration [7]. Besides, the spatial resolution of this measurement can be increased by selecting an appropriate ultrasonic transducer which helps gather localised information of the tissue region of interest. In fact, the PA tomography and microscopy instruments are designed for small animal studies by exploiting these advantages [7, 8].

There are some commercially available systems to monitor haematocrit noninvasively during cardiopulmonary bypass or hemodialysis, although they all require an extracorporeal blood circuit [9–14]. The use of the optoacoustic technique for noninvasive and continuous monitoring of total [Hgb] was proposed by several authors [15–17] and a laser optoacoustic system for in vitro and in vivo noninvasive monitoring of total [Hgb] was built to demonstrate that the optoacoustic technique could be potentially used for noninvasive, real-time and continuous monitoring of total [Hgb] with high accuracy [18].

In this paper, we concentrate to present a recently developed theoretical model describing the generation of PA field by a collection of absorbers [19, 20]. This model has been explored here to study as to how PA field would vary with blood SO_2 for different incident optical radiations. Further, the accuracy of the PA technique using two laser sources estimating blood SO_2 has also been evaluated.

Theoretical description

When an optical radiation illuminates an absorber, it absorbs the light energy and emits pressure waves due to thermoelastic expansion. The spatio-temporal variation of the generated pressure field can be expressed through a wave equation derived under the condition of thermal confinement (i. e. the emission of pressure waves occurs before the heat conduction starts) [21]. The solution of the time independent wave equation for a spherical absorber can easily be obtained using suitable boundary conditions (such as, the continuity of the pressure field and the normal component of particle velocity) and is given by [21],

$$p_f^{\text{single}}(r, k_f) = \frac{i\mu\beta I_0 v_s a^2}{C_P r} \frac{[\sin\hat{q} - \hat{q}\cos\hat{q}]e^{ik_f(r-a)}}{\hat{q}^2[(1-\hat{\rho})(\sin\hat{q}/\hat{q}) - \cos\hat{q} + i\hat{\rho}\hat{v}\sin\hat{q}]}. \quad (1)$$

Here, β, C_P and μ are the thermal expansion coefficient, isobaric specific heat and optical absorption coefficient for the absorbing medium with radius a, respectively. The dimensionless quantity $\hat{\rho}$ represents the density ratio, $\hat{\rho} = \rho_s/\rho_f$, where ρ_s and ρ_f are the densities for the absorbing and fluid medium, respectively. Similarly, $\hat{v} = v_s/v_f$, where v_s and v_f are the sound propagation speeds in these two media, respectively. Another dimensionless quantity $\hat{q}$ is defined as, $\hat{q} = \omega a/v_s = k_s a$, where ω is the modulation frequency of the incident optical radiation with intensity I_0. The acoustic wave numbers in the absorbing and fluid medium are denoted by k_s and k_f, respectively. The superscript single represents that only one PA source has been considered.

The PA field in the asymptotic region ($r \to \infty$) generated by a collection of spheres with identical properties can be expressed as [19, 20],

$$p_f^{\text{many}}(r, k_f) \approx \frac{i\mu\beta I_0 v_s a^2}{C_P r} \frac{[\sin\hat{q} - \hat{q}\cos\hat{q}]e^{ik_f(r-a)}}{\hat{q}^2[(1-\hat{\rho})(\sin\hat{q}/\hat{q}) - \cos\hat{q} + i\hat{\rho}\hat{v}\sin\hat{q}]} \times \sum_{n=1}^{N} e^{-i\mathbf{k}_f\cdot\mathbf{r}_n}. \quad (2)$$

Here, N is the number of absorbers present in the illuminated region and that is denoted by the superscript many. In (2), the linear superposition theory has been used to obtain the field generated by an ensemble of particles.

The corresponding time dependent PA field is given by,

$$p_f^{\text{many}}(r,t) \approx \frac{i\mu\beta F v_s a^2}{2\pi C_P r} \times \int_{-\infty}^{\infty} d\omega \frac{[\sin\hat{q} - \hat{q}\cos\hat{q}]e^{ik_f(r-a-v_f t)}}{\hat{q}^2[(1-\hat{\rho})(\sin\hat{q}/\hat{q}) - \cos\hat{q} + i\hat{\rho}\hat{v}\sin\hat{q}]} \times \sum_{n=1}^{N} e^{-i\mathbf{k}_f\cdot\mathbf{r}_n}, \quad (3)$$

where F is the fluence of the incident optical radiation. In this derivation, it has been assumed that the absorbers have been illuminated uniformly by a delta function heating pulse. Note that this is the expression of an analytic signal, whose real part provides the radio frequency (RF) signal and the corresponding, signal amplitude as a function of time can be evaluated from its magnitudes. Further, signal amplitude is linearly proportional to the absorption coefficient of an absorber.

Computer simulation

A Monte Carlo algorithm known as the random sequential adsorption (RSA) technique was used to simulate 2D tissue realizations containing nonoverlaping circles under periodic boundary conditions. Figure 1 demonstrates two possible tissue configurations, where each circle represents a cell. A smaller region of interest (ROI) is shown in Fig. 1 for clarity. However, a bigger ROI of $200 \times 200\ \mu m^2$ was considered and it was occupied by the red blood cells (RBCs) at a hematocrit, H = 0.40. Note that RBCs are the dominant PA sources in a blood sample. The cells were assumed to be suspended in blood plasma. The numerical values for various parameters are presented in Table 1 (first two columns).

Another important parameter, that controlled the strength of a PA signal, was the absorption coefficient of a cell. It was computed by evaluating the relationship, $\mu = c_{Hb\,O_2}\epsilon_{Hb\,O_2} + c_{Hb}\epsilon_{Hb}$. Here, $c_{Hb\,O_2}$ and c_{Hb} are the concentrations of oxy and deoxyhemoglobin molecules in a cell, respectively. There are ≈280 million hemoglobin molecules that are packaged in an erythrocyte and accordingly, the concentration becomes $\approx 5.34 \times 10^{-3}$ moles/l [20]. Moreover, $\epsilon_{Hb\,O_2}$ and ϵ_{Hb} represent the molar extinction coefficients for those molecules, respectively [22, 23]. The cellular oxygenation states of RBCs were assumed to be identical in a tissue and that also defined the blood SO_2. The estimated μ values corresponding to different blood SO_2 levels are given in Table 1 (three columns in the right).

The PA RF line were generated by evaluating the integration in (3) numerically for the 600 and 1,064 nm incident laser wavelengths. The signal envelope histogram as well as power spectrum averaged over 200 lines were obtained from 200 different tissue configurations for each SO_2 level. The mean amplitudes obtained from simulated RF lines were also utilized to estimate blood SO_2 by computing the formula, $SO_2 = (P_{PA}^{\lambda_2}\epsilon_{Hb}^{\lambda_1} - P_{PA}^{\lambda_1}\epsilon_{Hb}^{\lambda_2})/(P_{PA}^{\lambda_1}\Delta\epsilon_{Hb}^{\lambda_2} - P_{PA}^{\lambda_2}\Delta\epsilon_{Hb}^{\lambda_1})$. Here, $P_{PA}^{\lambda_1}$ and $P_{PA}^{\lambda_2}$ denote the PA signal amplitudes for the incident optical radiations with wavelengths λ_1 and λ_2 and $\Delta\epsilon_{Hb} = \epsilon_{Hb\,O_2} - \epsilon_{Hb}$.

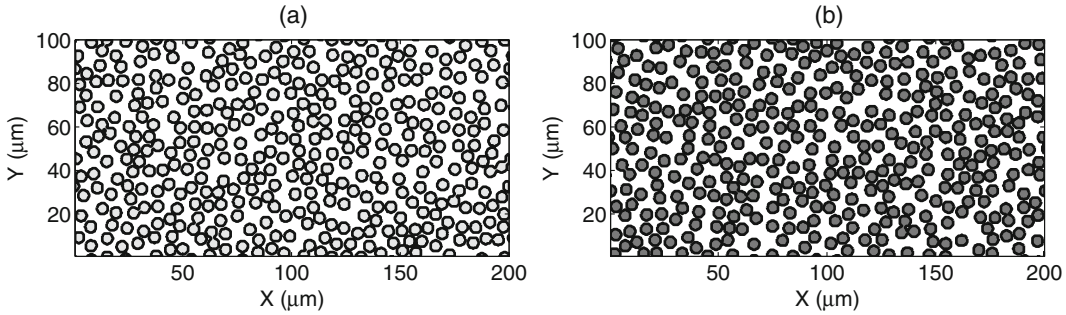

Fig. 1 2D simulated tissue realizations for blood $SO_2 = 50$ % in (**a**) and 100 % in (**b**)

Table 1 Numerical values for the parameters used in simulations (first two columns). Absorption coefficients for an erythrocyte at different blood SO_2 levels (three columns in the right)

Physical parameters		SO_2(%)	μ (m^{-1}) at 600 nm	μ (m^{-1}) at 1,064 nm
ROI	200×200 μm^2	0	18050.05	49.13
H	0.40	10	16638.58	85.01
N	673	20	15227.11	120.90
a	2.75 μm	30	13815.64	156.78
ρ_s	1,092 kg/m^3	40	12404.18	192.67
v_s	1,639 m/s	50	10992.71	228.55
ρ_f	1,021 kg/m^3	60	9581.24	264.44
v_f	1,547 m/s	70	8169.77	300.32
β	1 K^{-1}	80	6758.30	336.21
C_P	1 J $kg^{-1}K^{-1}$	90	5346.83	372.09
F	1 Jm^{-2}	100	3935.37	407.98

Simulation results

Figure 2a illustrates a typical PA RF line for the 600 nm laser source and $SO_2 = 50$ %. The time variation of the signal amplitude is also shown in Fig. 2a. Rapid variation of the signal amplitude can be observed from this figure and this is due to the presence of high frequency components. The envelope histogram averaged over 200 RF lines is presented in Fig. 2b. The Rayleigh distribution

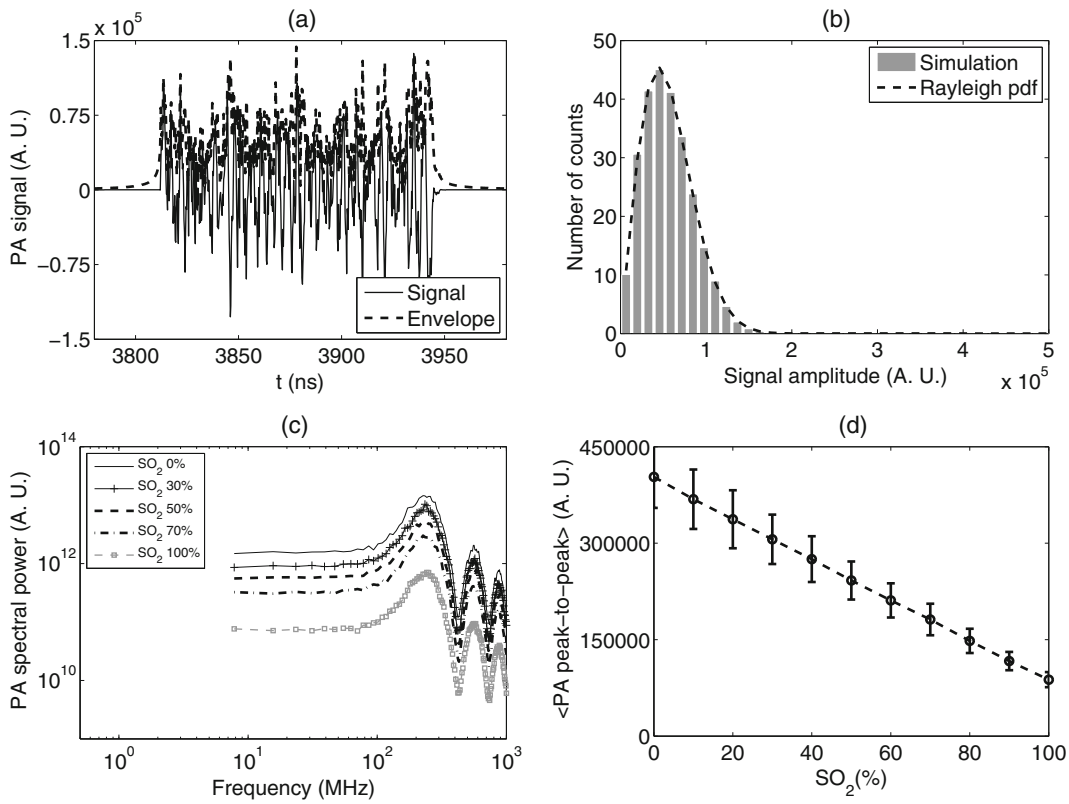

Fig. 2 **a** A computed RF line and its envelope for $SO_2 = 50$ % and the 600 nm laser source. **b** Plots of the envelope histogram averaged over 200 RF lines and the best fit Rayleigh distribution curve. **c** Variations of power spectral lines for some SO_2 levels. **d** Variation of the PA peak-to-peak amplitude with blood SO_2

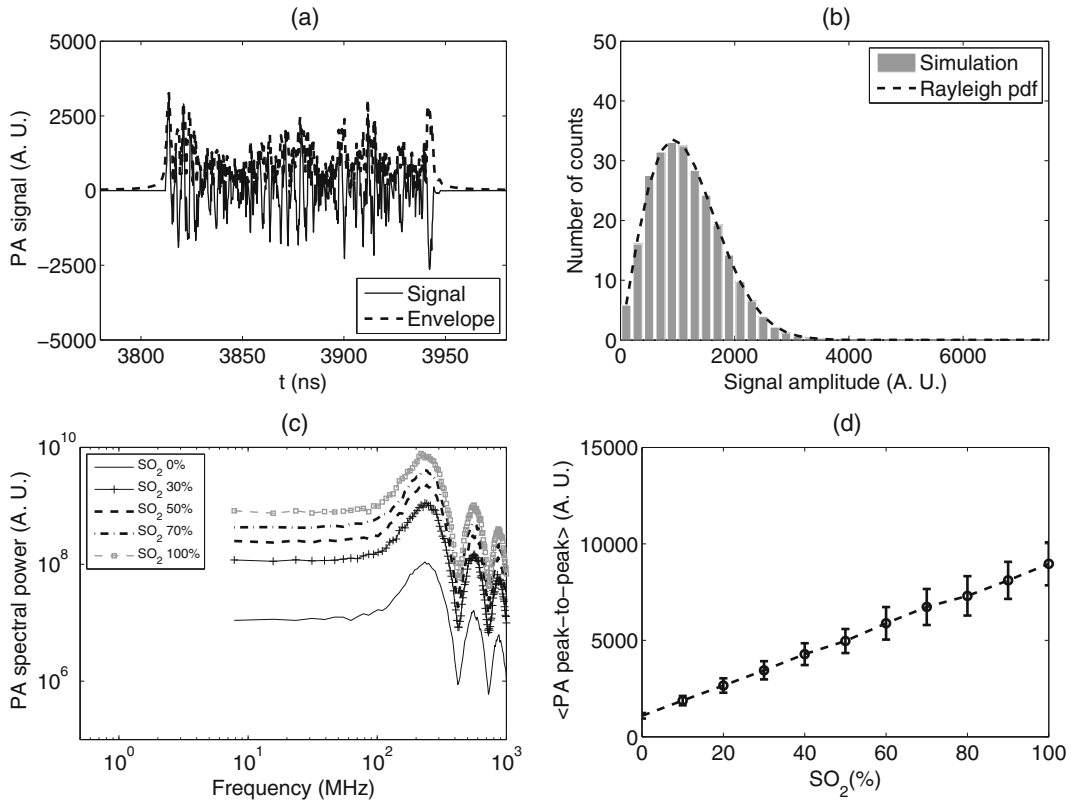

Fig. 3 **a** A typical RF line and its envelope for $SO_2 = 50$ % and the 1,064 nm laser source. **b** Plots of the envelope histogram averaged over 200 RF lines and the best fit Rayleigh distribution curve. **c** Variations of power spectral lines for some SO_2 levels. **d** Variation of the PA peak-to-peak amplitude with blood SO_2

provided a good fit to the histogram. The power spectral lines for some representative SO_2 levels are displayed in Fig. 2c over a wide range of frequencies (MHz to GHz). The spectral intensity decreases as the SO_2 increases. Each curve exhibits some dips that correspond to the minima of the Bessel function. In Fig. 2d, we have plotted the PA peak-to-peak amplitude as a function of blood SO_2 and it decreases linearly with blood SO_2. Note that the PA amplitude is nearly 4.6 times less at $SO_2 = 100$ % than that of 0 % and it is due to the fact that μ also varies in a similar manner (see Table 1).

A representative RF line and signal envelope are shown in Fig. 3a for the 1,064 nm laser source and $SO_2 = 50$ %. The signal amplitude has decreased significantly because μ in this case is lower than that of 600 nm. The envelope histogram along with the best fit Rayleigh distribution curve are displayed in Fig. 3b. The power spectral lines and variation of peak-to-peak amplitude with SO_2 are demonstrated in Fig. 3c and d, respectively. One can notice that the opposite trends are

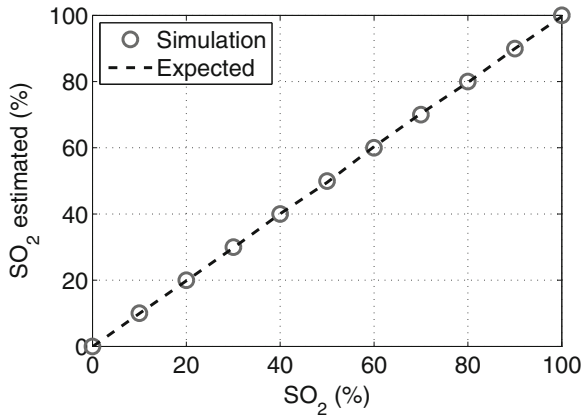

Fig. 4 Comparison between the estimated (using two laser radiations) and the actual SO_2

observed in this case than that of the previous case (Fig. 2c and d). This is expected because μ at 1,064 nm increases with the increasing concentration oxyhemoglobin molecules. Also, the PA amplitude is nearly 8.2 times higher at $SO_2 = 100$ % than that of 0 %.

The comparison between the estimated and the actual SO_2 is shown in Fig. 4. It appears that the estimated and true values are in excellent agreement.

Discussion and conclusions

A theoretical model is presented to describe the PA field generated by a collection of randomly located RBCs approximated as spheres at the same biophysical and biochemical conditions. The model has been utilized to investigate the effect of blood oxygen saturation on PA signal and thus the study deals with a forward problem. Note that to aid in the investigation of any novel optical methods for biological tissue characterization, accurate forward modeling is enormously useful for gaining physical insight, designing and optimizing experiments, as well as analyzing and interpreting the measured data.

In the derivation, it has been assumed that the multiple scattering of light is negligible and therefore RBCs at different spatial locations receive the same light intensity. This assumption is expected to be valid for a sparse medium. For a dense medium, attenuation of light beam due to multiple scattering becomes pronounced and consequently controls the fluence distribution reaching the light absorbing particles (i.e. RBCs). The attenuation of light beam needs to be incorporated while computing the PA signal using (3). The scattering and absorption coefficients together define the attenuation of light beam leading to the fact that its penetration and distribution of optical energy are wavelength dependent. As a result, apart from the oxygenation states of the Hb molecules, time domain profile of a PA signal appear to be greatly dependent on the incident optical radiation. Therefore, an appropriate part of the signal requires to be selected for accurate estimation of the tissue oxygen saturation.

Additionally, photons generally get multiply reflected from the cellular boundaries once they entire RBCs [24]. The multiple reflections of photons within the cells essentially increases the effective optical absorption of cells by enhancing the optical paths of photons. This phenomenon is optical wavelength dependent, and determines the PA emission strength. However, the present form of the model does not include this effect. Further, it has been reported in the literature that thermal diffusion can also contribute to the generation of PA signal [25]. The provision of generation of PA signals from such an origin has not been accounted in the theoretical framework presented in this article. In addition to that, the attenuation of the acoustic waves has been neglected in this model and it may become important particularly at higher ultrasound frequencies. If one works in the diagnostic frequency range, the attenuation is negligible, and does not affect the ultrasound frequency content of the signal significantly.

In this study, a Monte Carlo algorithm was implemented to simulate the tissue configurations. The algorithm implemented in this work generated spatial coordinates of the RBCs in such a way so that the cells would not overlap. The cells although are deformable but not penetrable which has been ensured during the generation of spatial coordinates of RBCs by applying the nonoverlapping condition. Tissue configurations with nonoverlapping cells can be thought to be a snap shot of a region of flowing blood under normal conditions. This simple approach was successfully utilized in the past to generate tissue configurations and explain various experimental results [19, 20]. It can be noted that the simulation approach may become unsuitable for blood samples with pathologies. For example, tissue realizations for aggregated blood samples, for which RBCs form clusters, cannot be mimicked using this algorithm.

In conclusion, it was observed that the PA signal amplitude decreased and increased linearly with blood SO_2 for the 600 and 1,064 nm laser sources, respectively. Similar observation has also been made experimentally. For example, measured PA signal amplitude exhibited a linear decrease and increase at the 700 and 1,064 nm, when the blood SO_2 varied from $\approx$20 to 95 % (Fig. 3

in [17]). Further, an excellent agreement between the estimated and actual blood SO_2 was observed confirming that the PA technique could be implemented in practice to assess blood oxygenation.

References

1. A. Zauner, E.M. Doppenberg, J.J. Woodward, S.C. Choi, H.F. Young, R. Bullock, Continuous monitoring of cerebral substrate delivery and clearance: initial experience in 24 patients with severe acute brain injuries. Neurosurgery **41**, 1082–1093 (1997)
2. R.O. Esenaliev, I.V. Larina, K.V. Larin, D.J. Deyo, M. Motamedi, D.S. Prough, Optoacoustic technique for noninvasive monitoring of blood oxygenation: a feasibility study. Appl. Opt. **41**, 4722–4731 (2002)
3. D.S. Prough, V. Yancy, D.J. Deyo, Brain monitoring: considerations in patients with craniocerebral missile wounds. in *Missile Wounds of the Head and Neck*, eds. by B. Aarabi, H.H. Kaufman (The American Association of Neurosurgical Surgeons, Rolling Meadows, III., 1999), pp. 221–253
4. S. Wray, M. Cope, D.T. Deply, J.S. Wyatt, E.O.R. Reynolds, Charaterization of the near infrared absorption spectra of cytochrome aa3 and hemoglobin for the non-invasive monitoring of cerebral oxygenation. Biochim. Biophys. Acta **933**, 184–192 (1988)
5. A.J. Welch, M.J.C. Van Gemert, *Optical-Themal Response of Laser-Irradiated Tissue* (Plenum, New York, 1981)
6. V. Pollard, D.S. Prough, Cerebral oxygenation: near-infrared spectroscopy. in *Principles and Practice of Intensive Care Monitoring*, ed. by M.J. Tobin (McGraw-Hill, New York, 1988), pp. 1019–1033
7. L.V. Wang, Prospects of photoacoustic tomography. Med. Phys. **35**, 5758–5767 (2008)
8. H.F. Zhang, K. Maslov, G. Stoica, L.V. Wang, Functional photoacoustic microscopy for high resolution and noninvasive in vivo imaging. Nat. Biotechnol. **24**(7), 848–851 (2006)
9. R.R. Steuer, D.A. Bell, L.L. Barret, Optical measurement of haematocrit and other biological constituents in renal therapy. Adv. Renal Replace. Ther. **6**, 217–224 (1999)
10. T. Kajiume, Y. Kawano, Y. Takaue, T. Abe, Y. Okamoto, A. Makimoto, T. Watanabe, J. Sato, A. Yokobayashi, Y. Kuroda, Continuous monitoring of haematocrit values during apheresis for allogeneic peripheral blood stem cell collection. J. Hematother. **7**, 493–497 (1998)
11. S.M. Yaskulka, J. Burnside, D. Bennett, V. Olshove, J. Langwell, Accuracy of in-line venous saturation and haematocrit monitors in pediatric perfusion. J. Extra-Corpor. Technol. **27**, 132–136 (1995)
12. S. Niles, R. Cronbaugh, J. Engle, J. Ploessl, R. Sutton, Evaluation of five in-line venous saturation and haematocrit monitors. J. Extra-Corpor. Technol. **27**, 24–28 (1995)
13. M.E. Brown, J.D. Rawleigh, J.M. Gallagher, In vitro evaluation of continuous mixed venous oxygen saturation and haematocrit monitors. J. Extra-Corpor. Technol. **26**, 189–193 (1994)
14. A. al Odeh, Z.A. Varga, G.D. Angelin, Haematocrit measurements during cardiopulmonary bypass surgery: comparison of three stat methods with a blood cell counter. Perfusion **9**, 127–134 (1994)
15. D.S. Prough, Y.E. Petrov, M.H. Klasing, M. Motamedi, R.O. Esenaliev, Continuous noninvasive optoacoustic monitoring of haemoglobin concentration: in vitro validation. Anesthesiology **95**, A555 (2001)
16. D.J. Deyo, R. Esenaliev, O. Hartrumpf, M. Motamedi, D.S. Prough, Continuous noninvasive optoacoustic monitoring of haemoglobin concentration: in vitro validation. Anesth. Analg. **92**, S139 (2001)
17. H.P. Brecht, Y.Y. Petrov, D.S. Prough, D.J. Deyo, O. Hartrumpf, R.O. in *Esenaliev, Noninvasive Continuous Optoacoustic Monitor of Total Haemoglobin Concentration*. Proceedings of the Second Joint EMSBS/BMES Coference, Institute of Electrical and Electronics Engineerings (Piscataway, N.J., 2002), pp. 2289–2290
18. R.O. Esenaliev, Y.Y. Petrov, O. Hartrumpf, D.J. Deyo, M. Motamedi, D.S. Prough, Coninous, noninvasive monitoring of total haemoglobin concentration by an optoacoustic technique. Appl. Opt. **43**, 3401–3407 (2004)
19. R.K. Saha, M.C. Kolios, A simulation study on photoacoustic signals from red blood cells. J. Acoust. Soc. Am. **129**, 2935–2943 (2011)
20. R.K. Saha and M.C. Kolios, Effects of erythrocyte oxygenation on optoacoustic signals. J. Biomed. Opt. **16**, 115003 (2011)
21. G.J. Diebold, in *Photoacoustic Monopole Radiation: Waves from Objects with Symmetry in One, Two and Three Dimensions*, ed. by L.V. Wang. Photoacoustic Imaging and Spectroscopy, chapter 1 (Taylor & Francis Group, London, 2009), pp. 3–17
22. Tabulated data from various sources complied by S. Prahl at http://omlc.ogi.edu/spectra. Accessed 10 March 2011
23. Y. Nomura, M. Tamura, Quantitative analysis of the hemoglobin oxygenation state of rat brain in vivo by picosecond time-resolved spectrophotometry. J. Biochem. **109**, 455–461 (1991)
24. A. Roggan, M. Friebel, K. Dörschel, A. Hahn, G. Müller, Optical properties of circulating human blood in the wavelength range 400–2500 nm. J. Biomed. Opt. **4**(1), 36–46 (1999)
25. I.G. Calasso, W. Craig, G.J. Diebold, Photoacoustic point source. Phys. Rev. Lett. **86**(16), 3550–3553 (2001)